



A photochemical synthesis route to typical transition metal sulfides as highly efficient cocatalyst for hydrogen evolution: from the case of NiS/g-C₃N₄

Hui Zhao^{a,1}, Huizhen Zhang^{a,1}, Guanwei Cui^b, Yuming Dong^{a,*}, Guangli Wang^a, Pingping Jiang^a, Xiuming Wu^a, Na Zhao^a

^a Key Laboratory of Synthetic and Biological Colloids (Ministry of Education of China), School of Chemical and Material Engineering, Jiangnan University, Wuxi 214122, PR China

^b College of Chemistry, Chemical Engineering and Materials Science, Collaborative Innovation Center of Functionalized Probes for Chemical Imaging in Universities of Shandong, Shandong Normal University, Jinan 250014, PR China



ARTICLE INFO

Keywords:
Photocatalytic
Hydrogen evolution
Water splitting
Photochemical method
NiS/g-C₃N₄

ABSTRACT

Precise deposition of cocatalysts on the outlet points of photo-generated electrons is helpful for highly efficient photocatalytic hydrogen evolution. Up to now, photochemical preparation of hydrogen production cocatalysts composed of earth-abundant elements is still great challenging and rarely reported. Herein, from the case of NiS/g-C₃N₄, a general photochemical synthesis route to typical transition metal sulfides as cocatalyst for hydrogen evolution was proposed. NiS were prepared by a facile and rapid photochemical method. The content of deposited NiS can be simply adjusted by the change of irradiation time. The optimized photocatalytic hydrogen evolution rate mounted up to 16 400 μmol g⁻¹ h⁻¹ with 0.76 wt% NiS loading, which is about 2500 times higher than that of pure g-C₃N₄. The photocatalytic H₂ evolution rate was stable after 40 h. The turnover number (TON) reached 1230 000 in 52 h with a turnover frequency (TOF) of 23 600 for NiS. Furthermore, the hydrogen evolution of the NiS/g-C₃N₄ composite photocatalyst reached 28.3 mmol g⁻¹ during 7 h under natural sunlight. The presence of NiS cocatalyst can efficiently promote the separation of photogenerated electron-hole pairs of g-C₃N₄, which was supported by the steady-state photoluminescence spectroscopy and photoelectro-chemical analyses.

1. Introduction

As the energy dilemma and environmental pollution problems become increasingly serious, the development of green renewable energy has attracted widespread attention. Hydrogen has the advantages of high combustion value and recycling clean, which is considered to be the most desirable green energy of the 21st century and can be used as a substitute for fossil fuels. Photocatalytic hydrogen evolution via water splitting is one of the promising and valuable strategies for converting inexhaustible solar energy into available chemical energy [1–3]. Though lots of photocatalysts have been reported and studied [4–6], research on low cost, high-efficiency, good-durability and solar-driven photocatalysis materials is still a hot topic.

The composite photocatalysts are usually made up of a photosensitizer and a cocatalyst to the H₂ evolution reaction (HER). Layered C₃N₄ with a similar graphitic structure (g-C₃N₄) has been reported as a metal-free polymer n-type semiconductor with the advantages of good sunlight absorption property ($E_g = 2.7$ eV) and photocatalytic stability

for water splitting [7–11]. However, the photocatalytic activity of pure g-C₃N₄ is low due to its fast recombination of photogenerated electron-hole pairs. Cooperating with cocatalyst is an effective way to facilitate the charge separation of the photogenerated electron-hole pairs for g-C₃N₄ [12,13]. However, to date, the reported cocatalysts used in previous studies are mainly noble metals, such as Pt, Au and Pd [14–16], which are rare and expensive. To reduce the cost of photocatalytic H₂ production, there is an important interest in introducing highly effective and inexpensive noble-metal-free cocatalyst into g-C₃N₄ [17–21].

In recent years, typical transition metal sulfides such as nickel sulfides have been identified as promising candidate electrocatalysts for enhancing hydrogen evolution [22–24]. It is well agreed that employing an electrocatalyst as a cocatalyst to accelerate the photocatalytic hydrogen evolution reaction on the semiconductor surface [25,26]. In addition, nickel sulfides were composed of two earth-abundant element. Therefore, it is highly expected that nickel sulfides can be used as promising cocatalysts resulting in the enhancement of light-driven hydrogen evolution performance of g-C₃N₄. Since 2013,

* Corresponding author.

E-mail address: dongym@jiangnan.edu.cn (Y. Dong).

¹ These authors contributed equally.

several nickel sulfides/g-C₃N₄ composite photocatalysts have been synthesized by various methods, representing excellent performance for hydrogen production from water, including NiS/mesoporous C₃N₄ and NiS₂/g-C₃N₄ (hydrothermal method) [26,27], NiS/g-C₃N₄ (ion-exchange method) [28], NiS/e-C₃N₄ (precipitation and hydrothermal method) [29]. These great works indicated promising application of nickel sulfides as photocatalytic HER cocatalysts. However, up to now, all the reported nickel sulfides in photocatalytic systems are linked or mixed randomly with photo-active materials. As known, transferring photo-generated electrons to protons is the main work of HER cocatalyst, and the charge transfer will be influenced obviously by the position cocatalyst loaded. Therefore, the connective point between cocatalyst and photo-active materials is desirable to be located at the electron outlet points of photo-active materials. As a result, the design of precise preparation strategy to couple nickel sulfides with the outlet points of photo-generated electrons on g-C₃N₄ is of great significance.

Photochemical synthesis is a mild and rapid approach to prepare cocatalyst on photo-active substances. Recently, many studies have demonstrated that noble metals can be precisely deposited on the outlet points of photo-generated electrons by photochemical route, which is of advantage to the charge transfer and helpful for efficient and stable hydrogen evolution [30–32]. However, up to now, photochemical synthesis of HER cocatalyst composed of noble-metal-free elements is still rare and challenging [17,33,34]. To the best of our knowledge, photo-reduction deposition of earth-abundant typical transition metal sulfides such as Co and Ni sulfides has not been reported.

Taking above conditions into consideration, herein, a general photochemical synthesis route to typical transition metal sulfides as cocatalyst for hydrogen evolution was proposed from the case of NiS/g-C₃N₄ (as shown in Scheme 1). When the preparation time was 20 min, the highest photocatalytic hydrogen evolution rate mounted up to 16400 μmol g⁻¹ h⁻¹. The turnover number (TON) reached 1230 000 in 52 h with a turnover frequency (TOF) of 23 600 for NiS. As far as we know, this is one of the most robust g-C₃N₄ based HER photocatalysts using transition metal sulfides as cocatalysts. In addition, the general applicability of the photochemical synthesis route was proved by expanding NiS to CoS and g-C₃N₄ to CdS.

2. Experimental section

2.1. Materials

Thiourea (CH₄N₂S, 99.0%), triethanolamine (C₆H₁₅NO₃, 98.0%), nickel acetate (C₄H₆NiO₄·4H₂O, 98.0%), cobalt acetate (C₄H₆CoO₄·4H₂O, 99.0%), absolute ethanol (C₂H₅OH), chloroplatinic acid hexahydrate (H₂PtCl₆·6H₂O, 37.0% Pt basis), cadmiumchloride (CdCl₂·2.5H₂O, 99.0%), ethylenediamine (H₂NCH₂CH₂NH₂, 99.0%) and sodium sulfate (Na₂SO₄, 99.0%) were purchased from Sinopharm Chemical Reagent Co. Ltd. Nafion® perfluorinated resin solution was purchased from sigma-aldrich. All reagents were used without further

purification.

2.2. Preparation of g-C₃N₄ nanosheets

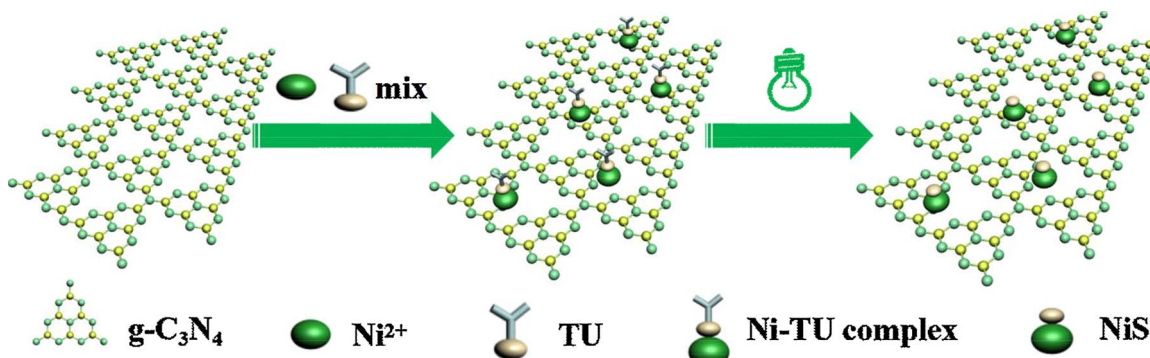
The g-C₃N₄ nanosheets were synthesized according to our previous report [18]. Briefly, 20 g thiourea was heated at 550 °C for 2 h in static air with a ramp rate of 2 °C min⁻¹. After that, the resultant yellow bulk g-C₃N₄ was milled into fine power, placed in an open porcelain crucible and heated at 500 °C with a heating rate of 2 °C min⁻¹ and maintained at this temperature for 2 h. Finally, light yellow powder (about 0.1 g) of g-C₃N₄ nanosheets was obtained.

2.3. Synthesis of NiS/g-C₃N₄ composites

The g-C₃N₄ nanosheets based NiS composite photocatalysts were prepared by a photochemical deposition method. In detail, 20 mg of g-C₃N₄ was added in a mixture solution of 1 mL Ni(CH₃COO)₂ aqueous solution (12.5 mg mL⁻¹), 1 mL thiourea aqueous solution (38 mg mL⁻¹), 4 mL ethanol and 4 mL ultrapure water. Subsequently, the resultant suspension was purged with nitrogen for 40 min to remove air. Irradiation was carried out for given period of time (0–30 min) with a 300 W Xenon lamp at room temperature to vary the deposition content of NiS. Finally, the grey products were collected centrifugation and washing repeatedly with water and alcohol, and dried in 60 °C vacuum oven. The acquired samples were denoted as NiS-T/g-C₃N₄, where T referred to the photochemical deposition time (min).

2.4. Characterization

X-ray diffraction (XRD) patterns were recorded on a D8 X-ray diffractometer (Bruker AXS, German). Transmission electron microscopy (TEM) and high resolution transmission electron microscopy (HRTEM) images were collected on a JEM-2100 transmission electron microscope (JEOL, Japan) to examine the morphology and size of sample. To detect surface species of sample, X-ray photoelectron spectroscopy (XPS) analysis was conducted using an ESCALAB 250 Xi (Thermo, USA) X-ray photoelectron spectrometer with Al K α line as the excitation source ($\hbar\nu = 1484.8$ eV) and adventitious carbon (284.8 eV for binding energy) was used as reference to correct the binding energy of sample. UV-vis diffuse reflectance spectra were measured on a UV-3600 (Shimadzu, Japan) spectrophotometer. Fourier transform infrared (FTIR) spectra were recorded by averaging 32 scans with a resolution of 2 cm⁻¹ using a Nicolet 6700 (Thermal, USA) infrared spectrometer with a DLaTGS detector. Atomic absorption spectrophotometry (Varian, USA Spectra AA-220/220Z) was used to detect the Ni element content in the sample. Photoluminescence spectra were recorded by using a fluorescence spectrophotometer (Cary Eclipse, Varian, USA). In order to explore the charges features, the surface photovoltage (SPV) spectra was measured by self-made equipment.



Scheme 1. Proposed photochemical synthesis route of NiS/g-C₃N₄.

2.5. Photocatalytic hydrogen production

The photocatalytic experiments were performed in a 50 mL flask at ambient temperature using a 300 W Xe lamp equipped with an AM 1.5 G filter. 5 mg of NiS/g-C₃N₄ composite was added in a mixture solution of 9 mL water and 1 mL triethanolamine. Before each experiment, the suspension was purged with pure nitrogen gas for 40 min to remove air. Hydrogen gas evolution was measured by gas chromatography (FULI GC9790 using a 5 Å molecular sieve column, argon as a carrier gas) with a thermal conductivity detector (TCD).

The turnover number (TON) and turnover frequency (TOF) were calculated by using the following equations:

$$\text{TON} = \frac{\text{moles of evolved H}_2}{\text{moles of NiS on photocatalyst}}$$

$$\text{TOF} = \frac{\text{TON}}{\text{reaction time(hours)}}$$

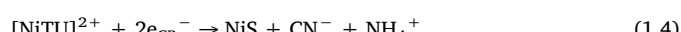
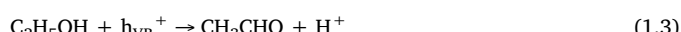
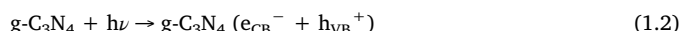
2.6. Photoelectrochemical measurements

Photocurrents were measured on a CHI600D electrochemical analyzer (Chenhua Instruments Co., Shanghai) in a standard three-electrode system with a working electrode, a Pt net as the counter electrode and Ag/AgCl as the reference electrode. A 300 W Xe lamp served as the light source. The electrolyte was 0.50 mol L⁻¹ Na₂SO₄ aqueous solution. The working electrode was prepared as follows: 2.0 mg of sample was dispersed in a mixture solution of 0.8 mL ethanol, 0.2 mL water and 40 μL Nafion® perfluorinated resin solution. 50 μL of resultant suspension was uniformly dropped onto a 1 × 1 cm² indium-tin oxide (ITO) glass. And then the electrode was dried at 60 °C for 12 h. The electrochemical impedance spectroscopy (EIS) frequency ranged from 0.1 to 100000 Hz in parallel with the alternating current signal amplitude of 5 mV.

3. Results and discussion

3.1. Photochemical formation of NiS/g-C₃N₄

When thiourea (TU) was mixed with Ni²⁺ ions, the [NiTU]²⁺ complex was generated (Eq. (1.1)) [35,36]. Due to the high specific surface area and the beneficial structure of the g-C₃N₄ nanosheet, the [NiTU]²⁺ complex can be effectively adsorbed on its surface. Under irradiation, the g-C₃N₄ adsorbed and harvested light to generate electron-hole pairs which were subsequently transported to the surface (Eq. (1.2)). Ethanol acted as a hole scavenger and was oxidized by the holes on the valence band to yield CH₃CHO and H⁺ (Eq. (1.3)) [37]. The photogenerated electrons accumulated in the g-C₃N₄ conduction band possessed enough reductive driving force to reduce the adsorbed [NiTU]²⁺ complex (Eq. (1.4)) leading to the production of a NiS/g-C₃N₄ hybrid photocatalyst.



Firstly, control experiments were carried out to illustrate the necessity of every precursor on the synthesis of NiS/g-C₃N₄. The specific experiment conditions were listed as shown in Table 1. After the initial formation course, five different solid catalysts from system A, B, C, D and E, were collected through further treatments, including centrifugation, washing and drying. Then the photocatalytic hydrogen evolution activity of them were tested under the same conditions, and the H₂ evolution rate were shown in Fig. 1. In experiment A, the

mixture including g-C₃N₄, Ni(CH₃COO)₂, TU and C₂H₅OH was treated for 20 min under UV-vis light, and this is a typical approach to synthesize NiS/g-C₃N₄, whose corresponding H₂ evolution rate (16400 μmol g⁻¹ h⁻¹) was much higher than that of several other tests. Compared with experiment A, the differences of the experiment B, C, D and E are the absence of Ni(CH₃COO)₂, TU, C₂H₅OH and irradiation, and the photocatalytic hydrogen evolution activity are 75 μmol g⁻¹ h⁻¹, 7047 μmol g⁻¹ h⁻¹, 4101 μmol g⁻¹ h⁻¹ and 1193 μmol g⁻¹ h⁻¹, respectively. What's more, after 20 min irradiation, there was no any precipitation formation in system F, indicating the unique role of photo-active material (g-C₃N₄). Consequently, these conditions including photo-active material, nickel salt, proper sulfur source, sacrifice agent and irradiation were all indispensable to prepare the NiS/g-C₃N₄ composite photocatalyst.

3.2. Characterization of NiS/g-C₃N₄

XRD patterns (Fig. S1) were used to investigate the phase structure of pure g-C₃N₄ and NiS/g-C₃N₄ composite photocatalyst. Both pure g-C₃N₄ and NiS/g-C₃N₄ had two distinct diffraction peaks at 28.0° and 13.1° which can be indexed to graphitic materials as the (002) and (100) planes of JCPDS 87-1526. These results illustrated that the g-C₃N₄ nanosheet structure maintained unchanged after NiS deposition. No NiS peaks were observed from the XRD patterns possibly due to the low content of NiS and the well dispersed NiS particles on the surface of g-C₃N₄.

FTIR spectra were used to study of chemical functional groups of pure g-C₃N₄ and NiS/g-C₃N₄ composite as presented in Fig. S2. The broad band located in 2850–3400 cm⁻¹ involving residual N–H components and O–H bands were associated with uncondensed amino groups and surface-adsorbed H₂O molecules. A broad adsorption band in the region between 790 and 1750 cm⁻¹ was related to the ploy-condensation structure of g-C₃N₄ which were attributed to the vibration characteristic of s-triazine ring units and heptazine heterocyclic ring units [38]. Pure g-C₃N₄ and NiS/g-C₃N₄ composite photocatalyst had similar absorption bands which indicated that the introduction of NiS did not change the structure of g-C₃N₄. These results were in good accordance with XRD analyses.

TEM and HRTEM images were used to observe the morphology and composition of a typical NiS-20/g-C₃N₄ photocatalyst, and the results were given in Fig. 2. From the TEM image (Fig. 2a), it was founded that NiS particles with sizes of several to tens of nanometers were deposited on the surface of g-C₃N₄ nanosheets. HRTEM image (Fig. 2b) presented an interplanar spacing of about 0.321 nm and 0.201 nm, which corresponded to the (002) lattice plane for g-C₃N₄ and the (102) lattice plane for NiS, respectively [17,29]. These results further confirmed the successful deposition of NiS particles on the surface of the g-C₃N₄ nanosheets.

XPS spectra were recorded to analyze the surface species and chemical states for NiS-20/g-C₃N₄. Fig. 3a presents the high resolution XPS spectrum of C1s in which the peak at 284.8 eV was due to the adsorbed carbon species on the surface and the 288.2 eV peak was ascribed to the network of g-C₃N₄ [39]. As displayed in the high resolution XPS spectrum of N 1s (Fig. 3b), three deconvolution peaks at 398.6, 399.2 and 400.9 eV should be assigned to the sp²N atoms in the triazine units, bridging N in N-(C)₃ of N–H and N in the heterocycles and cyano groups, respectively [40]. The binding energy of the main peak of Ni 2p was found at 855.4 eV in Fig. 3c, which was consistent with that of Ni²⁺ 2p_{3/2} in NiS [41]. Fig. 3d gave the high resolution XPS spectrum of S 2p. The peak at 162.8 eV corresponded to the S²⁻ [42]. The 168.0 eV peak was likely due to the thiourea dimerization product thioperoxydicaronimidic diamide [43]. In addition, the Ni content in NiS-20/g-C₃N₄ was determined by atomic absorption spectrophotometry and the ratio of NiS/g-C₃N₄ was calculated as 0.76 wt%. These results were in good agreement with the generation of NiS on the g-C₃N₄ surface.

Table 1
Preparation conditions for control experiments.

$\text{g-C}_3\text{N}_4/\text{mg}$	$\text{Ni}(\text{CH}_3\text{COO})_2 (12.5 \text{ mg mL}^{-1})/\text{mL}$	$\text{Thiourea (38 mg mL}^{-1})/\text{mL}$	$\text{C}_2\text{H}_5\text{OH}/\text{mL}$	$\text{H}_2\text{O}/\text{mL}$	Irradiation/min
A 20	1	1	4	4	20
B 20	0	1	4	5	20
C 20	1	0	4	5	20
D 20	1	1	0	8	20
E 20	1	1	4	4	Dark 20
F 0	1	1	4	4	20

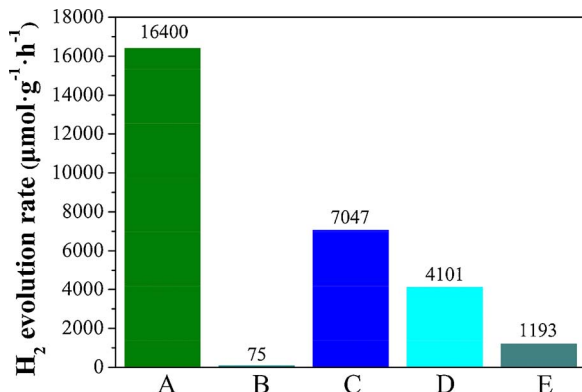


Fig. 1. Comparison of the photocatalytic H_2 evolution activity of sample A, B, C, D and E obtained by the control experiments in Table 1. The system contains 5.0 mg photocatalyst, 1 mL TEOA (98%) and 9 mL water. The light source was a 300 W Xe lamp with an AM 1.5G cut-off filter.

3.3. Photocatalytic performance

The photocatalytic H_2 production activity of $\text{NiS/g-C}_3\text{N}_4$ with different photochemical deposition time was investigated as shown in Fig. S3. At first, the H_2 production significantly enhanced with the increase of the preparation time. When it was 20 min, the highest photocatalytic activity mounted up to $16\ 400 \mu\text{mol g}^{-1} \text{h}^{-1}$, which is about 2500 times higher than that of pure $\text{g-C}_3\text{N}_4$ ($6.5 \mu\text{mol g}^{-1} \text{h}^{-1}$). These results indicated that pure pristine $\text{g-C}_3\text{N}_4$ was not active for photocatalytic H_2 evolution and NiS was an effective cocatalyst for $\text{g-C}_3\text{N}_4$. Longer preparation time resulted in decrease of the photocatalytic activity and the H_2 evolution rates were reduced to $14813.0 \mu\text{mol g}^{-1} \text{h}^{-1}$ (25 min) and $12024.3 \mu\text{mol g}^{-1} \text{h}^{-1}$ (30 min) respectively, which was possibly due to the overloading NiS shield $\text{g-C}_3\text{N}_4$ from light harvesting [44,45]. Since platinum has been used to enable extraordinary performance for photocatalytic H_2 production, we prepared and measured the hydrogen evolution activity of 0.76 wt% $\text{Pt/g-C}_3\text{N}_4$ for comparison under the

same conditions (Fig. S4). Photocatalytic activity of $\text{Pt/g-C}_3\text{N}_4$ reached $29\ 900 \mu\text{mol g}^{-1} \text{h}^{-1}$, which is higher than that of $\text{NiS/g-C}_3\text{N}_4$. However, the cost of noble metal Pt is far more than NiS. Therefore, NiS expects to serve as an alternative to precious platinum for photocatalytic hydrogen production.

In view of practical applications, besides catalytic activity, the stability and durability are also indispensable to photocatalysts. In order to evaluate the stability and durability of $\text{NiS-20/g-C}_3\text{N}_4$, we performed the time-circle H_2 evolution experiment. Fig. 4(a) presented the H_2 evolution as the function of irradiation time. The total photocatalytic H_2 amount of $\text{NiS-20/g-C}_3\text{N}_4$ after 52 h reaction was about 514 mmol g^{-1} and the turnover number (TON) reached 1230 000 in 52 h with a turnover frequency (TOF) of 23 600 for NiS. The photocatalytic H_2 evolution rate did not markedly decline after 10 runs for 40 h, indicating the good stability and durability of the $\text{NiS-20/g-C}_3\text{N}_4$ sample for photocatalytic H_2 production. After the 52 h cycling experiments, the H_2 generation rate dropped to about $7.0 \mu\text{mol g}^{-1} \text{h}^{-1}$, only 63% of the first cycle. The decrease of activity might be attributed to the slow fall-off of the NiS nanoparticles from $\text{g-C}_3\text{N}_4$ surfaces due to complex action with triethanolamine and Ni^{2+} . The next step for the research will be finding an effective solution to improve the stability of $\text{NiS/g-C}_3\text{N}_4$. It is to be observed that the H_2 production rate (after 52 h) is still far more than that of recently reported nickel sulfides/ $\text{g-C}_3\text{N}_4$ photocatalysts (Table S1). From what we can learn, the obtained $\text{NiS/g-C}_3\text{N}_4$ was one of the best transition metal sulfides modified $\text{g-C}_3\text{N}_4$ photocatalytic hydrogen production systems.

The ultimate goal of a photocatalyst can be capable of high-efficiency application of sunlight and solar energy. Therefore, H_2 evolution was also conducted with $\text{NiS-20/g-C}_3\text{N}_4$ photocatalyst under direct sunlight outdoors (Fig. S2). As illustrated in Fig. 4(b), the H_2 production quickly increased with the prolongation of sunlight irradiation time. During 7 h, the H_2 evolution reached 28.3 mmol g^{-1} , which indicated that $\text{NiS-20/g-C}_3\text{N}_4$ was also an efficient catalyst for sunlight-driven H_2 evolution from water. Such heterostructures may be expected to be promising candidates as effective sunlight photocatalysts and potential technological applications. After 16:00, the photocatalytic hydrogen

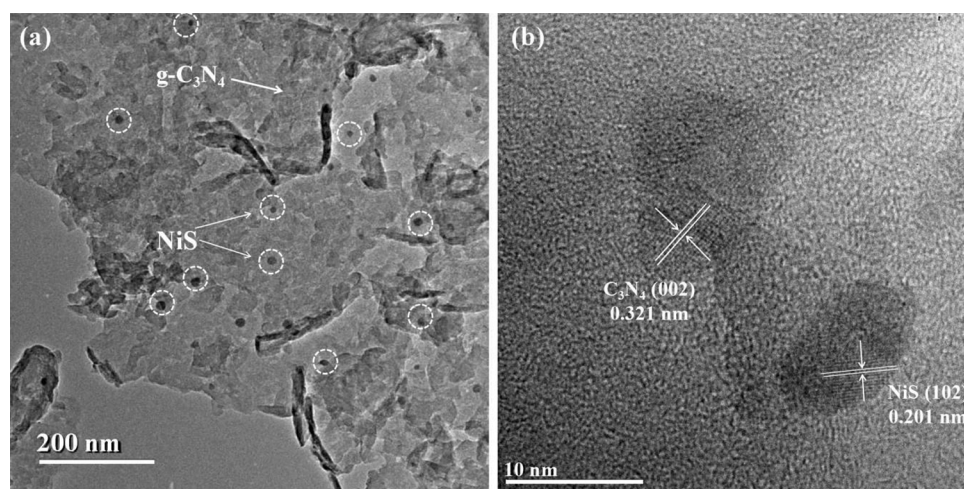


Fig. 2. (a) TEM image and (b) HRTEM image of $\text{NiS-20/g-C}_3\text{N}_4$.

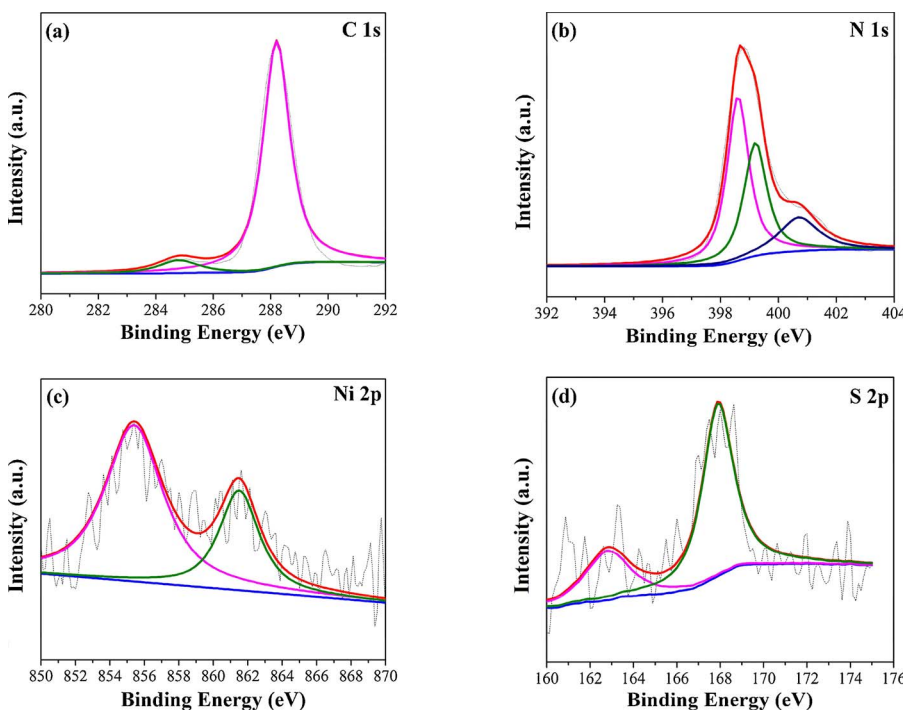
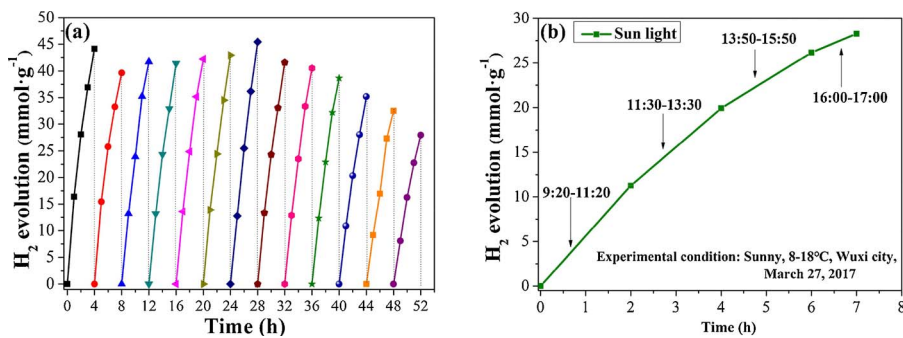


Fig. 3. High-resolution XPS spectra of C 1s (a), N 1s (b), Ni 2p (c) and S 2p (d) for NiS/g-C₃N₄.



evolution rate started to decline significantly assigned to solar dimming.

3.4. Proposed photocatalytic mechanism

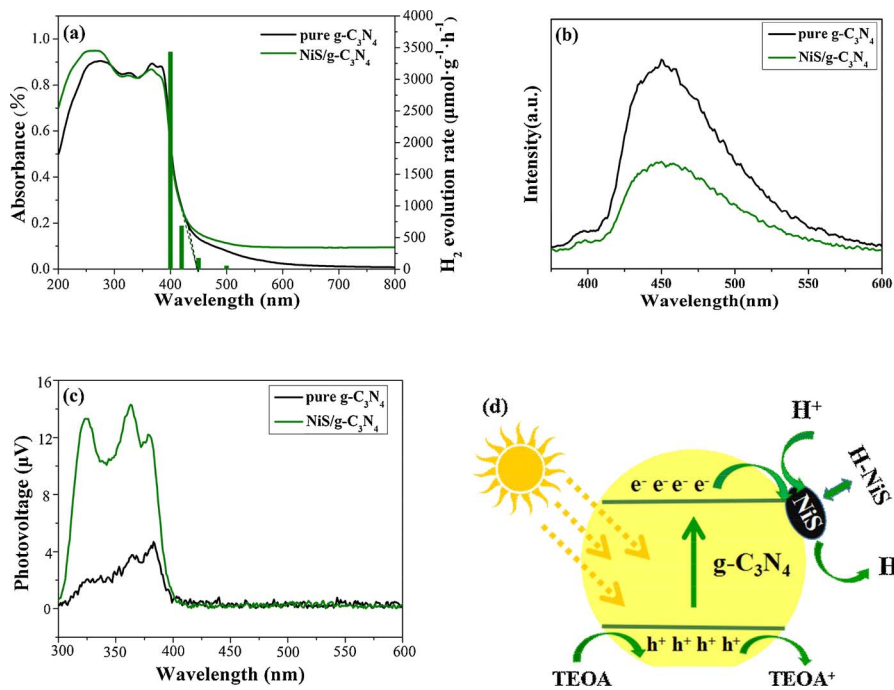
The UV-vis diffuse reflection spectra of pure g-C₃N₄ and NiS/g-C₃N₄ hybrid photocatalyst were recorded. As shown in Fig. 5(a), the pure g-C₃N₄ had an absorption edge at about 450 nm which corresponded to band gap of 2.71 eV for g-C₃N₄. When NiS was introduced, the NiS/g-C₃N₄ showed the same absorption edge as pure g-C₃N₄, indicating neither Ni nor S doping in the g-C₃N₄ structure. However, in comparison with pure g-C₃N₄, a broader absorption in the visible region was observed for NiS/g-C₃N₄ composite photocatalyst. Besides that, in order to identify whether the enhanced absorption of visible light was contribute positively to the remarkable photocatalytic activity of the NiS/g-C₃N₄, control experiments were carried out and the results are shown in Fig. 5(a). The photocatalytic H₂ evolution activity at different wavelengths were consistent well with the UV-vis absorption spectrum of pure g-C₃N₄, not that of NiS/g-C₃N₄. The results indicated that the enhanced absorption in the visible region from nickel sulfide was almost ineffective for its high activity. Given all that, the NiS played the part of the cocatalyst in this photocatalytic system.

Beyond this, photoluminescence (PL) emission spectra and surface photovoltage spectra (SPV) were performed to study the charge recombination and transfer behavior of the NiS/g-C₃N₄ composite.

Fig. 4. (a) Cycling runs for photocatalytic hydrogen evolution in the presence of 5.0 mg NiS-20/g-C₃N₄ photocatalyst in a 10 vol% aqueous triethanolamine solution, using a 300 W Xe lamp with an AM 1.5 G cut filter as the light source. After every 4 h, the produced H₂ was evacuated and 1 mL sacrificial agent (TEOA) was renewed. (b) Photocatalytic hydrogen production during 7 h under sunlight irradiation in Wuxi city on March 27, 2017. Experimental condition: Outdoor temperature: 8–18 °C, Time: 9:20–17:00. The system contains 5.0 mg NiS-20/g-C₃N₄, 1 mL TEOA (98%) and 9 mL water.

Fig. 5(b) gave the PL spectra of pure g-C₃N₄ and NiS/g-C₃N₄ with an excitation wavelength of 325 nm. Both pure g-C₃N₄ and NiS/g-C₃N₄ showed an emission peak at about 455 nm corresponding to the band gap for the recombination of photogenerated electrons and holes [18]. However, the PL emission intensity of g-C₃N₄ obviously decreased after loading NiS, suggesting that the charge recombination can be efficiently prevented for g-C₃N₄ after the NiS modification. As shown in Fig. 5(c), both pure g-C₃N₄ and NiS-20/g-C₃N₄ exhibited obvious positive photovoltage response with a wavelength between 300–400 nm, which match well with the photo-active wavelength range of the g-C₃N₄. Then the photovoltage values are almost zero in the range of 400–600 nm, and this means that the light of this wave band is invalid for both pure g-C₃N₄ and NiS/g-C₃N₄. These results showed that the band gap of g-C₃N₄ was not changed after loading of NiS and the NiS took the role of cocatalyst of the g-C₃N₄, which were consistent with the conclusions obtained from Fig. 5(a). Moreover, it was apparent that the photovoltage response intensity of the g-C₃N₄ improved significantly after the loading of NiS, demonstrating higher charge separation efficiency for the NiS/g-C₃N₄ compared to the native g-C₃N₄.

In the light of the contents mentioned above, the proposed photocatalytic H₂ production mechanism in NiS/g-C₃N₄ composite system was presented, as shown in Fig. 5(d). Under irradiation, g-C₃N₄ was excited and the electrons and holes then generated. However, in pure g-C₃N₄, the photogenerated carriers tended to recombine. According to above TEM and HRTEM results, it could be observed that g-C₃N₄ had an



intimate contact with NiS particles. In NiS/g-C₃N₄ composite, the photogenerated electrons in conduction band of g-C₃N₄ can easily transfer to NiS which prevented the recombination of photogenerated electrons and holes of g-C₃N₄. In this process, the intermediate H-NiS first formed by the absorption-reduction of one H⁺ for NiS (Eq. (2.1)), and then H₂ was electrochemically released by the reduction of another H⁺ (Eq. (2.2)). Such the hydride-NiS has been experimentally and computationally confirmed in many NiS hydrotreating processes [46].



To verify the proposed mechanism, photoelectrochemical (PEC) I-t curves and EIS Nyquist plots were investigated to verify the enhanced efficiency of charge separation and support the proposed photocatalytic H₂ production mechanism. Fig. 6(a) presented the photoelectrochemical (PEC) I-t curves of pure g-C₃N₄ and NiS/g-C₃N₄ electrodes under intermittent light irradiation. Compared with pure g-C₃N₄, the NiS/g-C₃N₄ hybrid photocatalyst showed higher photocurrent density, which indicated the efficient photogenerated charge transfer between NiS and g-C₃N₄ in NiS/g-C₃N₄ composite. Beyond this, as shown in Fig. 6(b), the EIS Nyquist plots of pure g-C₃N₄ and NiS/g-C₃N₄ were performed, and the NiS/g-C₃N₄ displayed much smaller EIS arc radius than g-C₃N₄. The results suggests that the NiS loading can greatly reduce the force of the charge transfer and separation, thus dominantly improving the H₂ production activity.

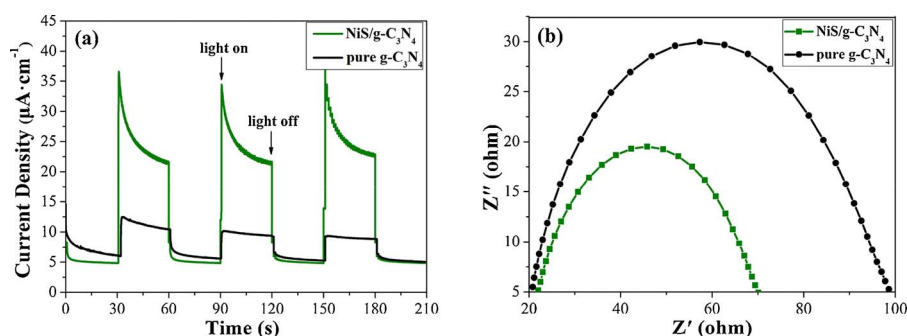


Fig. 5. (a) UV-vis-diffuse reflectance spectra of pure g-C₃N₄ and NiS-20/g-C₃N₄, and the H₂ evolution rate of NiS-20/g-C₃N₄. (The system contains 5.0 mg photocatalyst, 1 mL TEOA and 9 mL water, using a 300 W Xe lamp with different band-pass filters as the light source.). (b) Comparison of photoluminescence spectra of pure g-C₃N₄ and NiS-20/g-C₃N₄ composite. (c) surface photovoltage spectra of g-C₃N₄ and NiS-20/g-C₃N₄. (d) Proposed photocatalytic H₂ production mechanism in the NiS/g-C₃N₄ composite systems.

3.5. General applicability

In order to illustrate the general applicability of the photochemical synthesis route, a series of control experiments were carried out. Firstly, we changed NiS to CoS, and CoS-20/g-C₃N₄ was synthesized through a similar method. Photocatalytic HER rate of CoS-20/g-C₃N₄ came to 3732 μmol g⁻¹ h⁻¹, which was 574 times than that of native g-C₃N₄ (Fig. S6). Thus, it is fair to assume that different kinds of transition metal sulfides modified g-C₃N₄ photocatalysts can be synthesized via photochemical method and very likely possess outstanding H₂ evolution performance. In addition, to verify the applicability for photo-active materials, CdS and NiS-20/CdS were prepared and the photocatalytic activities were measured as shown in Fig. S7. To begin with, CdS nanorods were fabricated as in previous research [47], and the preparation process of the NiS-20/CdS NRs was no appreciable difference with the NiS/g-C₃N₄, only replacing g-C₃N₄ with CdS. The photocatalytic H₂ evolution rate of the CdS has received effective promotion after occupied the NiS. To sum up, this work provided a common strategy to built hydrogen production systems of transition metal sulfides modified semiconductor photosensitizers.

4. Conclusions

Taking NiS/g-C₃N₄ as a case, a novel photochemical synthesis route to typical transition metal sulfides was realized. The introduction of NiS on g-C₃N₄ surface significantly increased the photocatalytic H₂

Fig. 6. Comparison of transient photocurrent responses (a) and EIS Nyquist plots (b) of pure g-C₃N₄ and NiS/g-C₃N₄ composite.

evolution activity of g-C₃N₄ due to effective charge separation. The NiS-20/g-C₃N₄ showed the highest H₂ evolution activity of 16400 μmol g⁻¹ h⁻¹, and the photocatalytic H₂ evolution rate was not markedly decline after 40 h. The TON reached 1230 000 in 52 h with a TOF of 23 600 for NiS. Furthermore, the hydrogen evolution of the NiS-20/g-C₃N₄ composite photocatalyst reached 28.3 mmol g⁻¹ during 7 h under natural sunlight. NiS cocatalyst can efficiently promote the separation of photogenerated electron-hole pairs and consequently enhance the H₂ evolution activity of g-C₃N₄. This work opens a new door to precise preparation of typical transition metal sulfides for catalysis utilization.

Acknowledgements

The authors gratefully acknowledge the support from the National Natural Science Foundation of China (No. 21676123, 21575052), the Natural Science Foundation of Jiangsu Province (No. BK20161127), the Fundamental Research Funds for the Central Universities (JUSRP51623A), the Opening Foundation of Shandong Provincial Key Laboratory of Clean Production of Fine Chemicals (ZDSYS-KF201504) from Shandong Normal University and MOE & SAFEA for the 111 Project (B13025). The authors also thank Dr. Jinze Lv for his kind help on SPV technology.

Appendix A. Supplementary data

Supplementary data associated with this article can be found, in the online version, at <https://doi.org/10.1016/j.apcatb.2017.11.083>.

References

- [1] Z. Yu, Y. Xie, G. Liu, G. Lu, X. Ma, H. Cheng, J. Mater. Chem. A 1 (2013) 2773–2776.
- [2] Q. Wang, J. Li, Y. Bai, J. Lian, H. Huang, Z. Li, Z. Lei, W. Shangguan, Green Chem. 16 (2014) 2728–2735.
- [3] Y. Xie, Z. Yu, G. Liu, X. Ma, H. Cheng, Energy Environ. Sci. 7 (2014) 1895–1901.
- [4] X. Chen, S.S. Mao, Chem. Rev. 107 (2007) 2891–2959.
- [5] X. Chen, S. Shen, L. Guo, S.S. Mao, Chem. Rev. 110 (2010) 6503–6570.
- [6] D. Wang, L. Wang, A. Xu, Nanoscale 4 (2012) 2046–2053.
- [7] J. Zhang, X. Chen, K. Takanabe, K. Maeda, K. Domen, J. Epping, X. Fu, M. Antonietti, X. Wang, Angew. Chem. Int. Ed. 49 (2010) 441–444.
- [8] Y. Wang, X. Wang, M. Antonietti, Angew. Chem. Int. Ed. 51 (2012) 68–89.
- [9] X. Wang, S. Blechert, M. Antonietti, ACS Catal. 2 (2012) 1596–1606.
- [10] J. Chen, S. Shen, P. Guo, M. Wang, P. Wu, X. Wang, L. Guo, Appl. Catal. B 25 (2014) 335–341.
- [11] X. Bai, L. Wang, Y. Wang, W. Yao, Y. Zhu, Appl. Catal. B 25 (2014) 262–270.
- [12] S. Gao, J. Yu, J. Phys. Chem. Lett. 5 (2014) 2101–2107.
- [13] S. Zhang, J. Li, M. Zeng, J. Li, J. Xu, X. Wang, J. Chem. Eur. 20 (2014) 9805–9812.
- [14] D. Martin, K. Qiu, S. Shevlin, A. Handoko, X. Chen, Z. Guo, J. Tang, Angew. Chem. Int. Ed. 53 (2014) 9240–9245.
- [15] K. Maeda, X. Wang, Y. Nishihara, D. Lu, M. Antonietti, K. Domen, J. Phys. Chem. C 113 (2009) 4940–4947.
- [16] Y. Di, X. Wang, A. Thomas, M. Antonietti, ChemCatChem 2 (2010) 834–838.
- [17] J. Hong, Y. Wang, Y. Wang, W. Zhang, R. Xu, ChemSusChem (2013), <http://dx.doi.org/10.1002/cssc.201300647>.
- [18] H. Zhao, Y. Dong, P. Jiang, H. Miao, G. Wang, J. Zhang, J. Mater. Chem. A 3 (2015) 7375–7381.
- [19] J. Yu, S. Wang, B. Cheng, Z. Lin, F. Huang, Catal. Sci. Technol. 3 (2013) 1782–1789.
- [20] G. Zhang, G. Li, X. Wang, ChemCatChem 7 (2015) 2864–2870.
- [21] Y. Zhu, Y. Xu, Y. Hou, Z. Ding, X. Wang, Int. J. Hydrogen Energy 39 (2014) 11873–11879.
- [22] C. Tang, Z. Pu, Q. Liu, A.M. Asiri, X. Sun, Electrochim. Acta 153 (2015) 508–514.
- [23] D.Y. Chung, J.W. Han, D.H. Lim, J.H. Jo, S.J. Yoo, H. Lee, Y.E. Sung, Nanoscale 7 (2015) 5157–5163.
- [24] N. Jiang, Q. Tang, M. Sheng, Bo. You, D. Jiang, Y. Sun, Catal. Sci. Technol. 6 (2016) 1077–1084.
- [25] P.D. Tran, L.H. Wong, J. Barber, J.S.C. Loo, Energy Environ. Sci. 5 (2012) 5902–5918.
- [26] J. Hong, Y. Wang, Y. Wang, W. Zhang, R. Xu, ChemSusChem 6 (2013) 2263–2268.
- [27] L. Yin, Y. Yuan, S. Cao, Z. Zhang, C. Xue, RSC Adv. 4 (2014) 6127–6132.
- [28] Z. Chen, P. Sun, B. Fan, Z. Zhang, X. Fang, J. Phys. Chem. C 118 (2014) 7801–7807.
- [29] Y. Lu, D. Chu, M. Zhu, Y. Du, P. Yang, Phys. Chem. Chem. Phys. 17 (2015) 17355–17361.
- [30] J. Zhu, F. Fan, R. Chen, H. An, Z. Feng, C. Li, Angew. Chem. Int. Ed. 127 (2015) 9239–9242.
- [31] R. Li, F. Zhang, D. Wang, J. Yang, M. Li, J. Zhu, X. Zhou, H. Han, C. Li, Nat. Commun. 4 (2013) 1432–1438.
- [32] L. Mu, Y. Zhao, A. Li, S. Wang, Z. Wang, J. Yang, T. Liu, R. Chen, J. Zhu, F. Fan, R. Li, C. Li, Energy Environ. Sci. 9 (2016) 2463–2469.
- [33] L. Kong, Y. Dong, P. Jiang, G. Wang, H. Zhang, N. Zhao, J. Mater. Chem. A 4 (2016) 9998–10007.
- [34] Y. Dong, L. Kong, G. Wang, P. Jiang, N. Zhao, H. Zhang, Appl. Catal. B Environ. 211 (2017) 245–251.
- [35] G.M.S. El-Bahy, B.A. El-Sayed, A.A. Shabana, Vib. Spectrosc. 31 (2003) 101–107.
- [36] G.A.A. Al-Hazmi, A.A. El-Zahhar, K.S. Abou-Melha, F.A. Saad, M.H. Abdel-Rhman, A.M. Khedr, N.M. El-Metwaly, J. Coord. Chem. 68 (2015) 993–1009.
- [37] H. Zhao, Y. Dong, P. Jiang, G. Wang, H. Miao, R. Wu, L. Kong, J. Zhang, C. Zhang, ACS Sustain. Chem. Eng. 3 (2015) 969–977.
- [38] J.R. Holst, E.G. Gillan, J. Am. Chem. Soc. 130 (2008) 7373–7379.
- [39] Y. Hou, Z. Wen, S. Cui, X. Guo, J. Chen, Adv. Mater. 25 (2013) 6291–6297.
- [40] S. Yang, Y. Gong, J. Zhang, L. Zhan, L. Ma, Z. Fang, R. Vajtai, X. Wang, P.M. Ajayan, Adv. Mater. 25 (2013) 2452–2456.
- [41] J. Wen, J. Xie, H. Zhang, A. Zhang, Y. Liu, X. Chen, X. Li, ACS Appl. Mater. Interfaces (2017), <http://dx.doi.org/10.1021/acsmami.7b02701>.
- [42] H. Zhao, Y. Dong, P. Jiang, X. Wu, R. Wu, Y. Chen, RSC Adv. 5 (2015) 6494–6500.
- [43] Y. Sun, C. Liu, D.C. Grauer, J. Yano, J.R. Long, P. Yang, C.J. Chang, J. Am. Chem. Soc. 135 (2013) 17699–17702.
- [44] X. Wang, G. Liu, Z. Chen, F. Li, L. Wang, G. Lu, H. Cheng, Chem. Commun. 23 (2009) 3452–3454.
- [45] Z. He, J. Fu, B. Cheng, J. Yu, S. Gao, Appl. Catal. B Environ. 205 (2017) 104–111.
- [46] M. Breysse, E. Furimsky, S. Kasztelan, M. Lacroix, G. Perot, Catal. Rev. 44 (2002) 651–735.
- [47] Z. Sun, H. Zheng, J. Li, P. Du, Energy Environ. Sci. 8 (2015) 2668–2676.